We are IntechOpen,
the world's leading publisher of
Open Access books
Built by scientists, for scientists

6,900
Open access books available

186,000
International authors and editors

200M
Downloads

154
Countries delivered to

Our authors are among the

TOP 1%
most cited scientists

12.2%
Contributors from top 500 universities

BOOK CITATION INDEX
CLARIVATE ANALYTICS
INDEXED

WEB OF SCIENCE™

Selection of our books indexed in the Book Citation Index
in Web of Science™ Core Collection (BKCI)

Interested in publishing with us?
Contact book.department@intechopen.com

Numbers displayed above are based on latest data collected.
For more information visit www.intechopen.com

Simulation of SISO and MIMO Multipath Fading Channels

Antonio Petrolino[1] and Gonçalo Tavares[2]
[1]*Instituto de Engenharia de Sistemas e Computadores - Investigação e Desenvolvimento,
INESC-ID, Lisbon*
[2]*INESC-ID and Instituto Superior Técnico, IST, Lisbon*
Portugal

1. Introduction

Accurate software simulation is an important step for testing mobile communication systems. It allows the evaluation of the system performance without the need for physical experiments. At an early testing stage, simulations are usually done considering transmissions over additive white Gaussian noise (AWGN) channels, which do not account for obstacles or motion between the transmitter (Tx) and the receiver (Rx). According to the AWGN channel model, only the thermal noise which comes from the receiver amplifiers and from many natural sources is considered and added to the transmitted signal. This means that the received signal is a copy of the transmitted signal embedded in Gaussian noise, whose intensity depends on the propagation scenario (including the amplifiers of the Tx and the Rx) and can be controlled in simulation by tuning the Gaussian process variance.

It is easy to understand that AWGN channel models do not capture the conditions of a real radio channel where the presence of obstacles between the Tx and the Rx causes multipath propagation and may lead to *frequency selective* channels. In this situation, several replicas of the transmitted signal get to the Rx antenna with different propagation delays. If these delays are not negligible compared to the transmission interval T_s, the attenuation caused by the channel in the frequency-domain is not constant and a distortion is introduced[1]. Moreover, if there is motion between the Tx and the Rx, the received signal may be affected by a time-domain multiplicative distortion called *fading*. This happens because, being the Rx in motion relative to the Tx, the propagation channel characteristics vary with time and their effect can be modeled as a time-domain distortion affecting the transmitted signal. By combining both the effects of multipath propagation and fading on a wireless transmission, the received signal baseband equivalent $r(t)$ may be expressed as

$$r(t) = \sum_{i=1}^{N(t)} \rho_i(t)e^{j\theta_i(t)}s(t - \tau_i(t)) + n(t) \tag{1}$$

where $s(t)$ is the transmitted signal baseband equivalent, $\rho_i(t)$ and $\theta_i(t)$ are the time-varying attenuation and phase shift respectively of the i-th path and $n(t)$ is a white Gaussian process

---

[1] Otherwise, when the propagation delays are negligible compared to the signal interval, the channel is said to be *flat*.

modeling thermal noise and noise added by the receiver amplifiers. Although in the case of time varying channels $N(t)$ and $\tau_i(t)$ are functions of the time, for the sake of simplicity, it is common in the literature to ignore the dependence on time of the number of significant paths and the propagation delays, that is to set $N(t) = N$ and $\tau_i(t) = \tau_i$. Eq. (1) can be rewritten as

$$
\begin{aligned}
r(t) &= \sum_{i=1}^{N} \rho_i(t) e^{j\theta_i(t)} s(t - \tau_i) + n(t) \\
&= \sum_{i=1}^{N} h_i(t) s(t - \tau_i) + n(t)
\end{aligned}
\tag{2}
$$

where $h_i(t) \triangleq \rho_i(t) e^{j\theta_i(t)}$. Eq. (2) represents the received signal in the case of transmission over a *frequency-selective* channel.

In the case of *flat* multipath channels a further simplification is possible since $\tau_i \cong \overline{\tau} \ll T_s \ \forall i$. Eq. (2) can be rewritten as

$$
r(t) = \sum_{i=1}^{N} h_i(t) \cdot s(t - \overline{\tau}) + n(t).
\tag{3}
$$

Moreover, if a large number of paths is considered i.e., $N \gg 1$, the central limit theorem can be applied to the sum in (3) leading to

$$
r(t) = h(t) \cdot s(t - \overline{\tau}) + n(t)
\tag{4}
$$

where $h(t) = h_R(t) + jh_I(t)$ is a complex Gaussian random process.

By comparing equations (2) and (4), it is clear that the *selectivity* in the frequency-domain requires the contribution of each path to be considered and that the fading process, being the combination of N complex processes, each modeling the fading affecting the corresponding propagation path, can not be approximated by a Gaussian random process.

As far as flat fading channels are concerned, a detailed description of the process $h(t)$ was derived by Clarke in 1968. According to the *model of Clarke* (Clarke, 1968), for a mobile-to-fixed channel, the fading quadrature components are independent each with the same autocorrelation function (ACF) given by (Pätzold, 2002)

$$
\mathcal{R}_{h_R}(\tau) = \mathcal{R}_{h_I}(\tau) = \mathcal{R}_h(\tau) = \frac{\sigma_h^2}{2} \cdot J_0(2\pi f_D \tau)
\tag{5}
$$

where σ_h^2 is the fading power, $J_0(\cdot)$ is the zero-order Bessel function of the first kind and f_D is the maximum Doppler frequency shift. Two other widely used statistics in channel modeling for the statistical characterization of a fading process are the level crossing rate (LCR) and the average fade duration (AFD) of the process. The LCR L_R is defined as the expected number of times per second that the envelope $|h(t)|$ crosses the threshold R in the positive direction. For Rayleigh fading, it is given as (Patel et al., 2005)

$$
L_R = \sqrt{2\pi} f_D \rho e^{-\rho^2},
\tag{6}
$$

where $\rho = R/\sqrt{\mathbb{E}[|h(t)|^2]}$ (here, $\mathbb{E}[\cdot]$ denotes expectation). The AFD T_R is defined as the expected value for the length of the time intervals in which the stochastic process $h(t)$ is below a given level R. For Rayleigh fading, it is given as (Patel et al., 2005)

$$
T_R = \frac{e^{\rho^2} - 1}{\sqrt{2\pi} f_D \rho}.
\tag{7}
$$

It is important to note that some characteristics of the fading process, like the amplitude probability density function (PDF), can change considerably depending on the propagation scenario. For example, when a line-of-sight path is not available it can be shown that the complex Gaussian process $h(t)$ in (4) has zero-mean. Consequently, the fading process envelope PDF follows a Rayleigh distribution. Otherwise, when a line-of-sight path is available, the Gaussian process $h(t)$ has non-zero-mean leading to a Rician distributed envelope. However, experience shows that often the hypotheses of the model of Clarke are not verified and the fading severity turns out to be different from Rayleigh or Rician. In such cases, distributions like Nakagami-m (Nakagami, 1960), Weibull (Weibull, 1951) or Hoyt (Hoyt, 1947) match more closely with real fadings (Vehicular Technology Society Committee on Radio Propagation, 1988).

Simulation of fading processes with Rayleigh and Rician fading envelopes has been extensively studied e.g., the sum-of-sinusoids (SoS) method proposed in (Jakes, 1974), the simulator based on the inverse fast Fourier Transform (IFFT) proposed in (Smith, 1975), the filtering method presented in (Komninakis, 2003) and the simulator based on the Karhunen-Loève (KL) expansion presented in (Petrolino et al., 2008a).

The first approach, proposed by Jakes in (Jakes, 1974) is limited to the simulation of the Clarke's model for which it has been developed. It is based on the representation of the received signal as a superposition of a finite number of sinusoids having equal amplitude and uniformly spaced angle of arrivals. Jakes' simulator has to be considered as *deterministic* (Pätzold et al., 1998), since the generated waves depend on parameters which, once chosen, remain fixed for the duration of the simulation run. The SoS method was improved in (Pop & Beaulieu, 2001), with the addition of random phases, with the goal of making the generated process wide sense stationary (WSS).

The second approach, named IFFT-based method, was proposed in (Smith, 1975) and extended in (Young & Beaulieu, 2000). With this method, in order to achieve a fading output with the desired ACF, two real sequences of zero-mean independent Gaussian random variables (rvs) are multiplied in the frequency-domain by the same frequency mask equal to the square root of the power spectral density (PSD) corresponding to the desired ACF. Then, the obtained sequences are added in quadrature and a complex IFFT is taken. Due to the linearity of the IFFT, the output is a time-domain Gaussian sequence with the desired ACF.

The third approach is known as filtering method and resorts to digital filtering of computer-generated independent Gaussian rvs by a filter whose magnitude frequency response is given by the square root of the desired PSD. Due to the linearity of the filtering operation, the filter output sequence is still Gaussian and has the desired ACF. A solution based on the combination of an infinite impulse response (IIR) filter with a nearly ideal interpolator is proposed in (Komninakis, 2003).

The last approach is based on the idea of expanding the complex random fading process as a modified KL expansion. Let $h(t)$ be a correlated zero-mean complex Gaussian random process in $0 < t < T_0$ whose quadrature components are independent each showing the same ACF. The process $h(t)$ can be represented by the series expansion (Van Trees, 1968)

$$h(t) = \lim_{L \to \infty} \sum_{l=0}^{L-1} h_l \phi_l(t) \tag{8}$$

where the set of functions $\{\phi_l(t)\}_{l=0}^{L-1}$ is the basis of the expansion and the $\{h_l\}_{l=0}^{L-1}$ are the expansion coefficients, that is the projections of the process $h(t)$ on the basis functions. The representation in (8) is known as the Karhunen-Loève expansion for the process $h(t)$

(Van Trees, 1968). Since $h(t)$ is a zero-mean complex Gaussian random process and the $\{\phi_l(t)\}_{l=0}^{L-1}$ are orthogonal, the $\{h_l\}_{l=0}^{L-1}$ are zero-mean, independent complex Gaussian rvs with variances $\{\sigma_l^2\}_{l=0}^{L-1}$. A possible expansion for the process $h(t)$ is achieved by setting the process $h(t)$ correlation matrix eigenvectors and eigenvalues as the basis functions $\{\phi_l(t)\}_{l=0}^{L-1}$ and the variances $\{\sigma_l^2\}_{l=0}^{L-1}$, respectively (Petrolino et al., 2008b). Inversely, in fading channel simulation we need to generate a correlated random process starting from the *a priori* knowledge of its ACF which is determined by the channel model being used. This can be achieved by following the approach proposed in (Petrolino et al., 2008a), where the $\{\phi_l(t)\}_{l=0}^{L-1}$ is imposed as a complete set of exponential functions, leading to a *modified* KL expansion. Due to the particular choice of the basis functions, the eigenvalues can be calculated for $l = 0, \ldots, L-1$, as (Petrolino et al., 2008b, eq. (9))

$$\sigma_l^2 = \int_{-T_0/2}^{T_0/2} \mathcal{R}_h(\tau) \cos\left(\frac{2\pi l \tau}{T_0}\right) d\tau. \tag{9}$$

This means that if we are able to calculate the integral in (9) for every l, then the process $h(t)$ may be synthesized by (8) using a set of L computer-generated independent zero-mean Gaussian rvs, with variances $\{\sigma_l^2\}_{l=0}^{L-1}$.
At this point a N-samples version $h[n]$ of the fading process $h(t)$ may be obtained by sampling the interval T_0 with sampling frequency $f_s = N/T_0$

$$h[n] = \sum_{l=0}^{L-1} h_l \cdot e^{j\frac{2\pi}{N}ln} \quad n = 0, \ldots, N-1 \tag{10}$$

where the $\{h_l\}_{l=0}^{L-1} \sim N(0, \{\sigma_l^2\}_{l=0}^{L-1})$ are independent Gaussian rvs. The dimension of the expansion basis is (Van Trees, 1968) $L = 2BT_0$ where B is the unilateral bandwidth of the process and T_0 its duration. Since $T_0 = NT_s$, the KL expansion dimension reduces to $L = 2BNT_s = \frac{2B}{f_s}N \leq N$, where the inequality follows from the sampling theorem. This means that $h_l = 0$ for $l \geq N$, so it is possible to rewrite (10) as

$$h[n] = \sum_{l=0}^{N-1} h_l \cdot e^{j\frac{2\pi}{N}ln} \quad n = 0, \ldots, N-1 \tag{11}$$

that is, $h[n]$ is the IDFT of the sequence $\{h_l\}_{l=0}^{N-1}$ and may be computed efficiently using the fast Fourier transform (FFT) algorithm. Note that simulators like (Young & Beaulieu, 2000), (Komninakis, 2003) and (Petrolino et al., 2008a) impose the desired ACF by linear transformations of Gaussian processes. By the properties of this class of processes, the Gaussian PDF is preserved. However, this is not the case with non-Gaussian processes. As a consequence, such simulators can not be directly used to generate autocorrelated non-Gaussian sequences like Nakagami-m, Weibull or Hoyt. Regarding Nakagami-m fading, simulators have been proposed in (Beaulieu & Cheng, 2001) and (Filho et al., 2007), both of which require already-correlated Rayleigh sequences which must be generated by existing simulators. In (Beaulieu & Cheng, 2001), the correlated Nakagami sequence is obtained by applying a double transformation to the Rayleigh sequence, while in (Filho et al., 2007), an uncorrelated Nakagami sequence is rearranged according to the Rayleigh sequence ranking in order to match the desired ACF.

An important class of systems which have gained success in the last years are multiple-input multiple-output (MIMO) systems. Consequently, MIMO fading channel simulators are increasingly required by MIMO designers for system performance evaluation and assessment. In MIMO systems, multi-element antenna arrays are used at both sides of a radio link and the communication occurs over N_{min} parallel channels, where N_{min} is the minimum of the number of Tx or Rx antennas (Gesbert et al., 2000). Due to finite antenna separation, a spatial correlation between the channels always exists and greatly affects the link capacity of MIMO systems (Wang, 2006). The MIMO channel spatial correlation can be described by a $MN \times MN$ correlation matrix. This matrix can be obtained in several ways depending on the reference model under consideration. In this chapter we will use the Kronecker Based Stochastic Model (KBSM) (Wang, 2006). According to the KBSM model, the spatial correlation matrix $\mathbf{S}_{MIMO}$ is obtained as

$$\mathbf{S}_{MIMO} = \mathbf{S}_{BS} \otimes \mathbf{S}_{MS} \qquad (12)$$

where $\mathbf{S}_{BS}$ is the $M \times M$ spatial correlation matrix at the BS, $\mathbf{S}_{MS}$ is the $N \times N$ spatial correlation matrix at the MS and $\otimes$ stands for the Kronecker product. For the referred reasons, a MIMO fading channel simulator must contemplate the possibility of generating random processes cross-correlated according to a spatial correlation structure determined by the used model. In general, the fading channel simulation can be divided in three tasks:

1. Choice of the most convenient fading channel model.

2. Generation of uncorrelated rvs with the desired PDF. This point will be discussed in Sections 2 and 3.

3. Imposition of the desired ACF to the generated sequence without affecting the initial PDF. This point will be analyzed in Section 4.

This chapter is organized as follows. Section 2 presents a technique for the generation of uncorrelated arbitrary jointly distributed phase and envelope processes. The proposed method is based on the two-dimensional extension of the Metropolis-Hastings (MH) algorithm (Hastings, 1970; Metropolis et al., 1953). Starting from jointly Gaussian random variate pairs, this method achieves the desired PDF by an acceptance-rejection (AR) algorithm whose probability of acceptance is set in a convenient way.

In Section 3, the two-dimensional MH algorithm is applied to the generation of Nakagami-m and Hoyt envelope fading processes.

Section 4 presents a method for inducing the desired correlation structure on wireless channel simulation processes. It will be shown that it can be used for simulating both the spatial correlation between the propagation channels for MIMO systems and the time-ACF in case of single-input single-output (SISO) systems. The procedure is based on the method proposed by Iman & Conover (IC) in 1982 (Iman & Conover, 1982). This method is able to induce a desired correlation matrix on an input matrix whose columns are random vectors with independent arbitrary marginal distributions (Petrolino & Tavares, 2010a), (Petrolino & Tavares, 2010b). The IC method is distribution-free, which means that it preserves the marginal PDF of the input sequences while inducing the desired correlation. This important feature enables the generation of sequences with arbitrarily distributed PDFs and arbitrary correlation matrix.

Section 5 presents simulation results obtained by applying the IC method to the simulation of MIMO and SISO channels. In the MIMO case the simulated spatial correlation matrices are compared with the targets, while in the SISO case the comparison is made between the target and the simulated time ACFs. In both cases, perfect preservation of the initial PDF is achieved. Finally, Section 6 concludes the chapter.

2. The Metropolis-Hastings algorithm

In this Section, we present a computational efficient and accurate method for simulating every type of fading (e.g. Nakagami-m, Weibull, Hoyt, etc.) starting from PDFs (e.g. Gaussian or Uniform distribution) which can be easily generated by known and efficient methods. This method is based on the Metropolis-Hastings algorithm (Hastings, 1970; Metropolis et al., 1953) with an AR sampling proposed by Tierney in (Tierney, 1994).

Consider now the problem of simulating a fading channel characterized by arbitrary jointly distributed envelope and phase. For this purpose, let $h(t) = x(t) + jy(t)$ be a complex fading process and let $h(t) = \rho(t)e^{j\theta(t)}$ be its representation in polar coordinates.

Two possible ways exist for generating $h(t)$: the first is the direct generation of the envelope and phase processes $\rho(t)$ and $\theta(t)$ respectively, the second is generating the IQ component processes $x(t)$ and $y(t)$. The first solution is attractive in the sense that the characterization of fading channels is usually done in terms of envelope and phase PDFs. However, in telecommunications, system testing is usually carried out by considering the transmission of the signal IQ components over the fading channel under consideration.

Recalling that the IQ components joint PDF $f_{XY}(x,y)$ and the phase-envelope joint PDF $f_{R,\theta}(\rho,\theta)$ are related by

$$f_{XY}(x,y) = \frac{f_{R,\Theta}(\rho,\theta)}{|J|} \tag{13}$$

where $|J|$ is the Jacobian of the transformation

$$x = \rho\cos\theta, \quad y = \rho\sin\theta \tag{14}$$

we conclude that if we are able to generate pairs of rvs (x_i, y_i) following the joint PDF $f_{XY}(x,y)$ in (13), then the phase-amplitude joint PDF will be the desired $f_{R,\Theta}(\rho,\theta)$. The main issue in simulating fading processes is that usually, the distribution $f_{XY}(x,y)$ does not belong to any family of well-known PDFs and can not be directly generated. Here, we propose a method which allows the efficient generation of rvs with arbitrary distribution.

Suppose we want to generate a set of N pairs $(x_1^{(i)}, x_2^{(i)})|_{i=1,\ldots,N}$ following an *arbitrary target joint density* $f(\cdot)$ whose analytical expression is known, and that we have pairs (y_1, y_2) from a *candidate-generating joint density* $h(\cdot)$ that can be simulated by some known, inexpensive method. After setting an arbitrary initial pair $(x_1^{(0)}, x_2^{(0)})$ for initializing the algorithm, the MH method can be summarized as follows (Chib & Greenberg, 1995):

- Repeat the following steps for $i = 0,\ldots,N-1$

- Generate (y_1, y_2) from $h(\cdot)$ and u from a uniform distribution $u \sim \mathcal{U}(0,1)$

- **IF** $u \leq \alpha$
  Set $(x_1^{(i+1)}, x_2^{(i+1)}) = (y_1, y_2)$

- **ELSE**
  Set $(x_1^{(i+1)}, x_2^{(i+1)}) = (x_1^{(i)}, x_2^{(i)})$

where $\alpha = \alpha[(x_1^{(n)}, x_2^{(n)}), (y_1, y_2)]$ is the (conditional) probability of accepting the candidate pair (y_1, y_2) given that the current pair is $(x_1^{(n)}, x_2^{(n)})$. This probability is usually called *probability of move* (Chib & Greenberg, 1995), because it represents the probability of the process

moving to a new state. When the MH algorithm was proposed, this probability was set to (Tierney, 1994)

$$\alpha = \min \left\{ \frac{f(y_1, y_2)}{f(x_1^{(i)}, x_2^{(i)})}, 1 \right\} \tag{15}$$

which means that the higher is the target PDF at the candidate pair, the higher is the probability to accept it. Here we use a modified version of the MH algorithm.

This modification has been discussed in (Tierney, 1994) and it is based on the idea of introducing an acceptance-rejection step for generating candidates for a MH algorithm. Pairs (y_1, y_2) are generated from $Kh(\cdot)$ until a pair satisfying $u < f(y_1, y_2)$, where $u \sim \mathcal{U}\{0, Kh(y_1, y_2)\}$, in obtained. The constant K is set such that $f(x_1, x_2) \leq Kh(x_1, x_2)$ for all (x_1, x_2) and controls the acceptance rate. According to this method, only those pairs for which the target density $f(\cdot)$ is high are accepted as candidates for the MH algorithm. Moreover, the probability of move α is set as follows. Let

$$\mathbf{C} = \{(a, b) : f(a, b) < Kh(a, b)\} \tag{16}$$

be the set where $Kh(a, b)$ *dominates* $f(a, b)$. Four possible cases occur and the probability α is set as follows (Chib & Greenberg, 1995):

- *Case (a)*: $(x_1^{(n)}, x_2^{(n)}) \in \mathbf{C}$ and $(y_1, y_2) \in \mathbf{C}$.
  In this case $Kh(\cdot)$ dominates $f(\cdot)$ for both the current and the candidate pair. This means that with higher probability both pairs belong to $Kh(\cdot)$ rather than to the target PDF $f(\cdot)$. In this case the algorithm always accepts the new pair i.e., $\alpha = 1$;

- *Case (b)*: $(x_1^{(n)}, x_2^{(n)}) \in \mathbf{C}$ and $(y_1, y_2) \notin \mathbf{C}$.
  In this case the current pair belongs with higher probability to $Kh(\cdot)$ rather than to $f(\cdot)$. Moreover, for the candidate pair, $f(\cdot)$ is higher than $Kh(\cdot)$. This means that the probability of belonging to the target density is higher for the candidate pair than for the current pair. Also in this case the algorithm always accepts the new one i.e., $\alpha = 1$;

- *Case (c)*: $(x_1^{(n)}, x_2^{(n)}) \notin \mathbf{C}$ and $(y_1, y_2) \in \mathbf{C}$.
  The probability of belonging to $f(\cdot)$ is higher for the current pair than for the candidate pair. This means that the transition to other states must be controlled. In this case the methods sets

$$\alpha = \frac{Kh(x_1^{(n)}, x_2^{(n)})}{f(x_1^{(n)}, x_2^{(n)})}.$$

  Note that the higher the value of the target density $f(\cdot)$ at the current pair, the lower the probability to accept the candidate pair;

- *Case (d)*: $(x_1^{(n)}, x_2^{(n)}) \notin \mathbf{C}$ and $(y_1, y_2) \notin \mathbf{C}$.
  Both the current and the candidate pair belong with higher probability to the target PDF $f(\cdot)$ rather than to the candidate $Kh(\cdot)$. Also in this case the probability of move depends on the target and the candidate densities. It is easy to understand that it must be set such it is in general higher than in the previous case. The method in this case sets

$$\alpha = \min \left\{ \frac{f(y_1, y_2) \cdot h(x_1^{(n)}, x_2^{(n)})}{f(x_1^{(n)}, x_2^{(n)}) \cdot h(y_1, y_2)}, 1 \right\}.$$

Note that the higher the product $f(x_1^{(n)}, x_2^{(n)}) \cdot h(y_1, y_2)$, the lower the probability of move.

Compared with the standard MH algorithm, this version of the algorithm provides a PDF with a better match with the target distribution. This is achieved by observing that the initial distribution support can be divided in two kind of zones, one producing good values with higher probability than the other. It is important to note that, contrary to the standard MH algorithm, this method will occasionally reject candidates if the process is at a pair $(x_1^{(n)}, x_2^{(n)}) \notin \mathbf{C}$ (Tierney, 1994). By keeping the same pair for a certain number of consecutive steps, Metropolis-based methods introduce in general correlation along the sampled series. This can be harmful if uncorrelated processes are required. Our goal in this paper is to generate uncorrelated fading processes with desired envelope and phase PDFs. In this way, distribution-free algorithms can be applied to the generated pairs for imposing the desired correlation if second order statistics specification is required. We got round this difficulty by applying a random shuffling to the generated sequence at the end of the algorithm.

3. Simulation of uncorrelated arbitrary jointly distributed phase and envelope processes with the MH algorithm

In this Section we will show some results obtained by applying the previously described MH algorithm to two different propagation scenarios. We simulated the IQ components of fading channels characterized by arbitrarily distributed envelope and phase processes. As required by the algorithm we deduced analytical expressions of the target IQ components joint PDF $f(\cdot)$ from results available in the literature. In both the following examples the candidate pairs (y_1, y_2) follow the bivariate joint Gaussian PDF. They are independent Gaussian rvs with zero-mean and the same variance σ^2, so that their joint PDF reduces to the product of their Gaussian marginal PDFs and is given by

$$h(y_1, y_2) = \frac{1}{2\pi\sigma^2} \exp\left(-\frac{y_1^2 + y_2^2}{2\sigma^2}\right). \tag{17}$$

The constant K introduced in equation (16) has been adjusted by experimentation to achieve an acceptance rate of about 50%.
A rv representing a realization of a fading process at a fixed instant of time is

$$C = X + jY \tag{18}$$

where X and Y are rvs representing the fading process IQ components and

$$R = \sqrt{X^2 + Y^2} \quad \Theta = \tan^{-1}(Y/X) \tag{19}$$

are the envelope and the phase of C respectively. From (14), since the Jacobian is $|J| = \rho$, we have that

$$f_{XY}(x, y) = \frac{f_{R,\Theta}(\rho, \theta)}{\rho}. \tag{20}$$

3.1 Nakagami-m fading
For Nakagami-m fading, the envelope PDF is given by the well-known formula (Nakagami, 1960)

$$f_R(\rho) = \frac{2m^m \rho^{2m-1}}{\Omega^m \Gamma(m)} \exp\left(-\frac{m\rho^2}{\Omega}\right), \rho \geq 0 \ m > \frac{1}{2} \tag{21}$$

where $\Omega = \mathbb{E}[R^2]$ is the mean power, $m = \Omega^2/V[R^2]$ is the Nakagami fading parameter ($V[\cdot]$ denotes variance) and $\Gamma(\cdot)$ is the Gamma function.

For independent I and Q components, the corresponding phase PDF has been obtained in (Yacoub et al., 2005) and is given by

$$f_\Theta(\theta) = \frac{\Gamma(m)|\sin(2\theta)|^{m-1}}{2^m \Gamma^2(m/2)}, \quad -\pi \le \theta < \pi. \tag{22}$$

Considering the envelope and the phase as independent rvs, we have

$$f_{R,\Theta}(\rho,\theta) = f_R(\rho) \times f_\Theta(\theta). \tag{23}$$

The substitution of (23) into (20) leads to

$$f_{XY}(x,y) = \frac{m^m|\sin(2\theta)|^{m-1}\rho^{2m-2}}{2^{m-1}\Omega^m \Gamma^2(m/2)} \exp\left(-\frac{m\rho^2}{\Omega}\right) \tag{24}$$

where $\rho = \sqrt{x^2 + y^2}$ and $\theta = \tan^{-1}(y/x)$. We applied the proposed method for the generation of 2^{20} pairs of rvs following (24) starting from independent jointly Gaussian rvs with zero mean and variance $\sigma^2 = \Omega/2m$. The target and the simulated joint PDF are plotted in Fig. 1(a) and 1(b) respectively. In Fig. 2(a) and 2(b) the simulated envelope and phase PDFs are plotted

(a) Theory   (b) Simulation
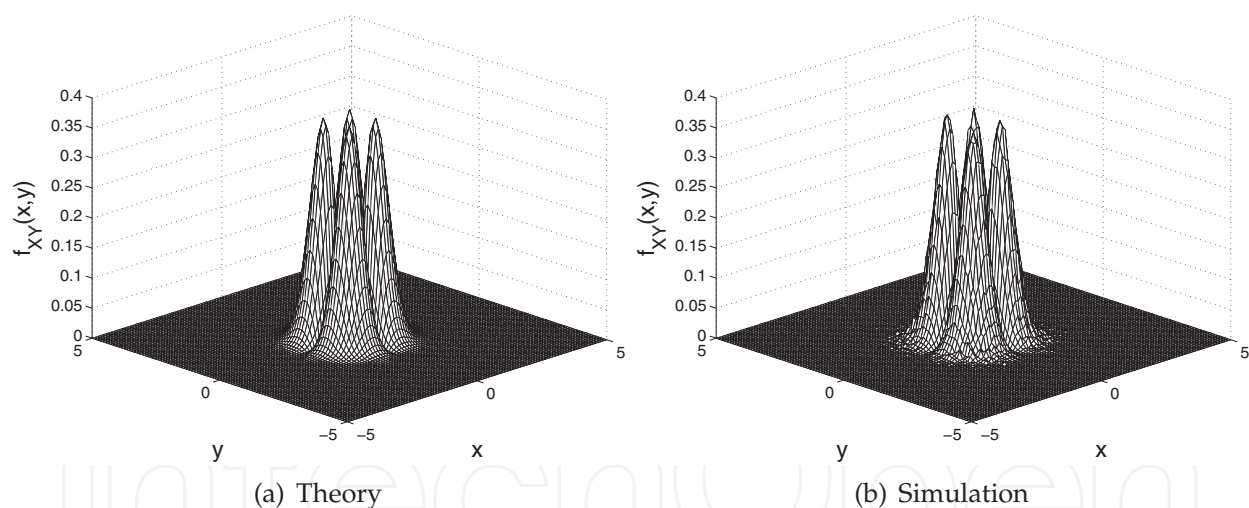
Fig. 1. Theoretical (a) and simulated (b) IQ components joint PDF for Nakagami-m fading with $m = 2$ and $\Omega = 1$.

respectively against the theoretical references. In both cases the agreement with the theory is very good. We now show how the application of a Metropolis-based method may introduce a (possibly not desired) correlation in the generated sequence and how this problem may be solved by random shuffling the sampled pairs. The correlation is due to the fact that until accepting a new candidate pair, the MH algorithm keeps the last pair as a good pair for sampling the target density $f(\cdot)$. However, the comparison of figures 3(a) and 3(b) shows that the (low) correlation introduced by the algorithm is completely canceled by the random shuffling.
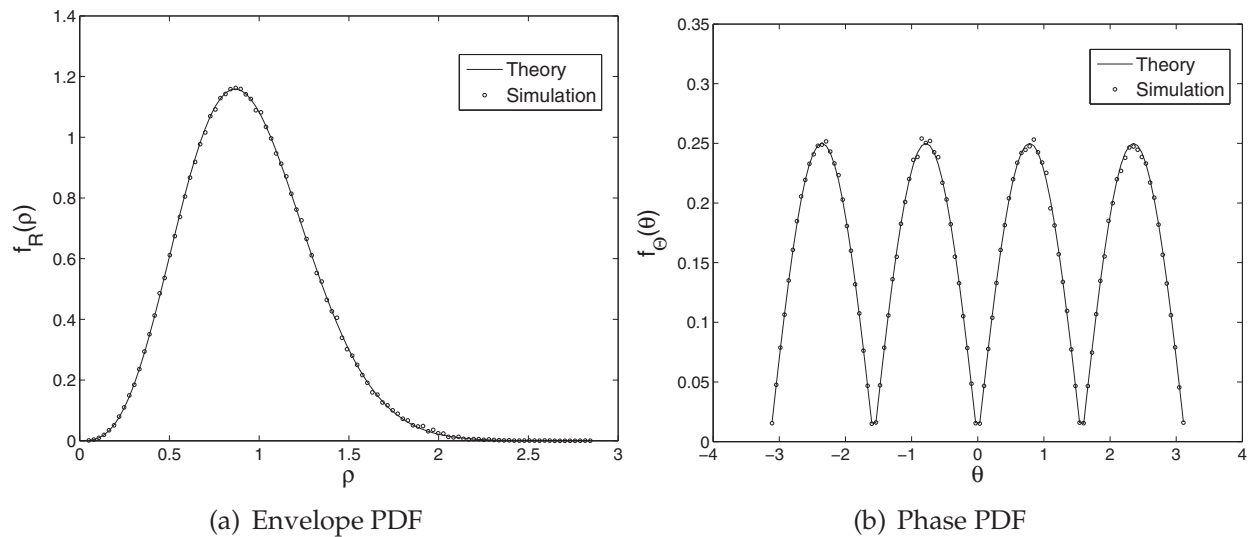
(a) Envelope PDF   (b) Phase PDF

Fig. 2. Simulated Nakagami-m envelope PDF (a) and phase PDF (b) plotted against theory for 2^{20} generated pairs, $m = 2$ and $\Omega = 1$.

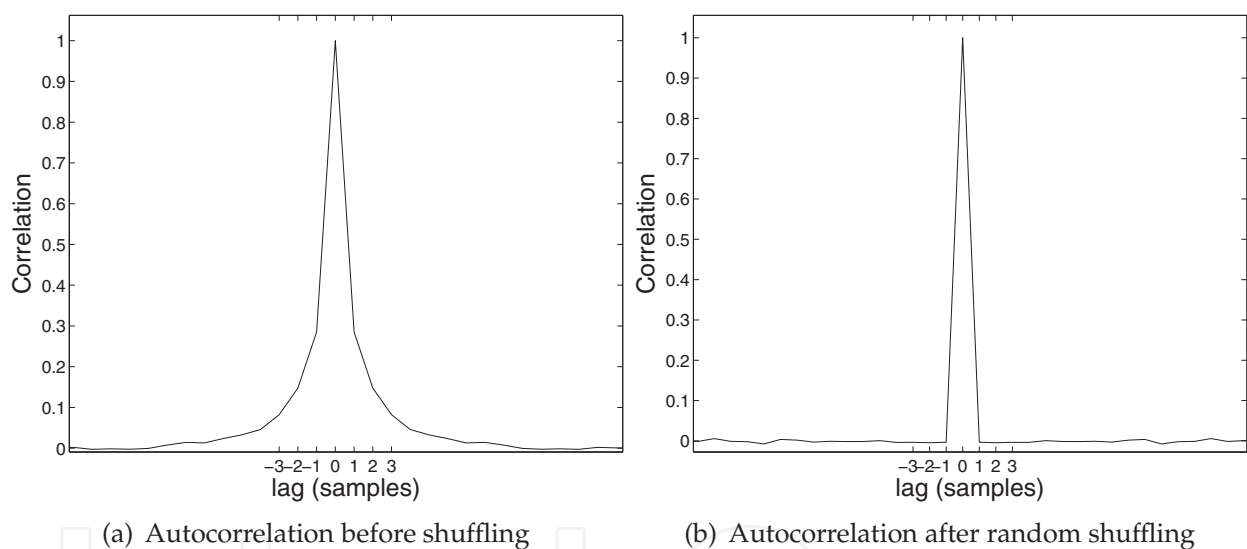(a) Autocorrelation before shuffling   (b) Autocorrelation after random shuffling

Fig. 3. Autocorrelation of the generated process in-phase component before (a) and after (b) the random shuffling.

3.2 Hoyt fading

For Hoyt fading, the envelope PDF is given by (Hoyt, 1947)

$$f_R(\rho) = \frac{2\rho}{\Omega\sqrt{1-b^2}} \exp\left(-\frac{\rho^2}{\Omega(1-b^2)}\right) \times I_0\left(\frac{b\rho^2}{\Omega(1-b^2)}\right), \quad \rho \geq 0 \tag{25}$$

where $\Omega = \mathbb{E}[R^2]$, $b \in [-1,1]$ is the Hoyt fading parameter and $I_0(\cdot)$ is the modified Bessel function of the first kind and zero-th order. The corresponding phase PDF is (Hoyt, 1947)

$$f_\Theta(\theta) = \frac{\sqrt{1-b^2}}{2\pi(1-b\cos(2\theta))}, \quad -\pi \leq \theta < \pi. \tag{26}$$

Considering also in this case independent envelope and phase processes and applying relation (20), we obtain the IQ components target joint PDF

$$f_{XY}(x,y) = \frac{1}{\Omega\pi(1 - b\cos(2\theta))}\exp\left(-\frac{\rho^2}{\Omega(1-b^2)}\right) \times I_0\left(\frac{b\rho^2}{\Omega(1-b^2)}\right) \qquad (27)$$

where $\rho = \sqrt{x^2 + y^2}$ and $\theta = \tan^{-1}(y/x)$. We applied the proposed method for the generation of 2^{20} pairs of rvs following (27) starting from independent jointly Gaussian rvs with zero mean and variance $\sigma^2 = \Omega(1 - b^2)/2$. The target and the simulated joint PDF are plotted in Fig. 4(a) and 4(b) respectively.

(a) Theory   (b) Simulation
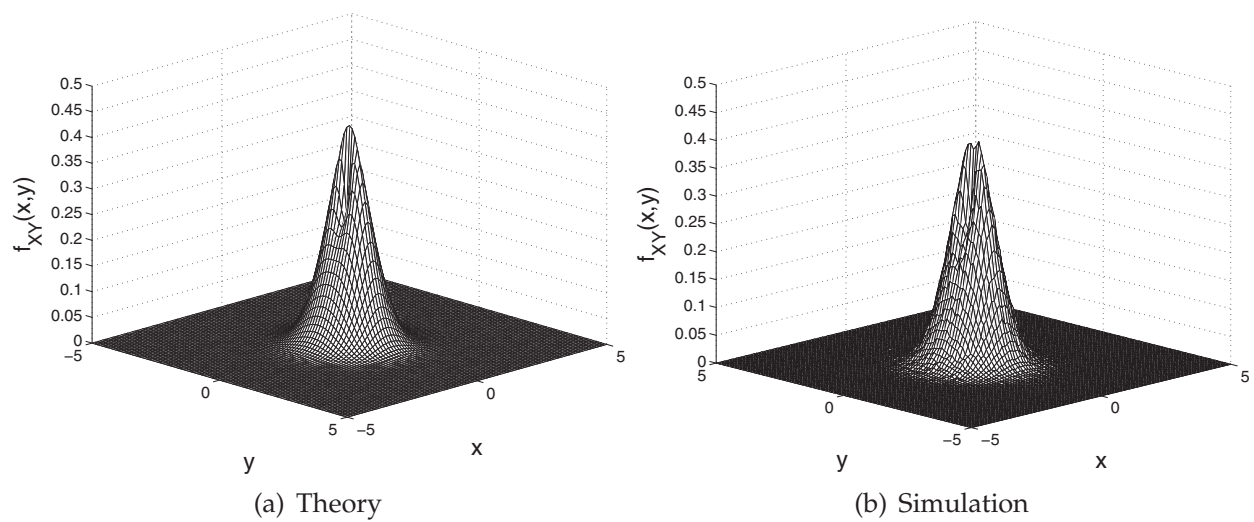
Fig. 4. Theoretical (a) and simulated (b) IQ components joint PDF for Hoyt fading with b=0.25 and $\Omega = 1$.

In Fig. 5(a) and 5(b) the simulated envelope and phase PDFs are plotted respectively against the theoretical references. Also in this case the agreement with the theory is very good.

4. The Iman-Conover method

Let us consider a $n \times P$ matrix $\mathbf{X}_{in}$, with each column of $\mathbf{X}_{in}$ containing n uncorrelated arbitrarily distributed realizations of rvs. Simply stated, the Iman-Conover method is a procedure to induce a desired correlation between the columns of $\mathbf{X}_{in}$ by rearranging the samples in each column. Let $\mathbf{S}$ be the $P \times P$ symmetric positive definite target correlation matrix. By assumption, $\mathbf{S}$ allows a Cholesky decomposition

$$\mathbf{S} = \mathbf{C}^T\mathbf{C} \qquad (28)$$

where $\mathbf{C}^T$ is the transpose of some $P \times P$ upper triangular matrix $\mathbf{C}$. Let $\mathbf{K}$ be a $n \times P$ matrix with independent, zero-mean and unitary standard deviation columns. Its linear correlation matrix $\mathbf{R}_{lin}(\mathbf{K})$ is given by

$$\mathbf{R}_{lin}(\mathbf{K}) = \frac{1}{n}\mathbf{K}^T\mathbf{K} = \mathbf{I} \qquad (29)$$

where $\mathbf{I}$ is the $P \times P$ identity matrix. As suggested by the authors in (Iman & Conover, 1982), the so-called "scores matrix" $\mathbf{K}$ may be constructed as follows: let $\mathbf{u} = [u_1 \dots u_n]^T$ denote the
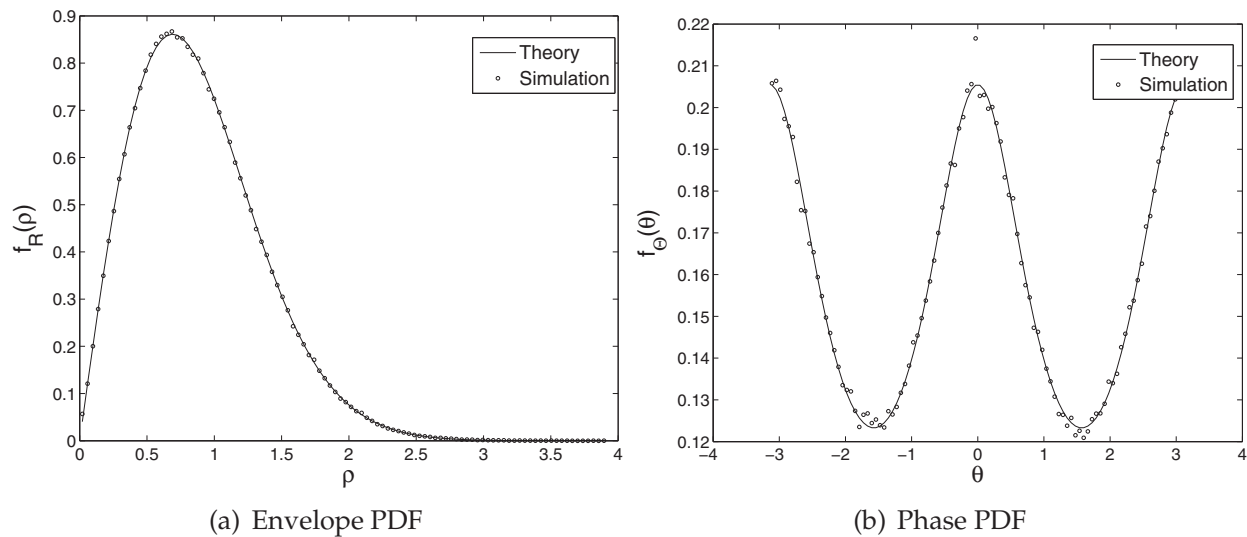
(a) Envelope PDF   (b) Phase PDF

Fig. 5. Simulated Hoyt envelope PDF (a) and phase PDF (b) plotted against theory for 2^{20} generated pairs, $b = 0.25$ and $\Omega = 1$.

column vector with elements $u_i = \Phi^{-1}(\frac{i}{n+1})$, where $\Phi^{-1}(\cdot)$ is the inverse function of the standard normal distribution function, then $\mathbf{K}$ is formed as the concatenation of P vectors

$$\mathbf{K} = \frac{1}{\sigma_{\mathbf{u}}}[\mathbf{u}\ \mathbf{v}_1\ \ldots\ \mathbf{v}_{P-1}] \tag{30}$$

where $\sigma_{\mathbf{u}}$ is the standard deviation of $\mathbf{u}$ and the $\mathbf{v}_i$ are random permutations of $\mathbf{u}$. The columns of $\mathbf{K}$ have zero-mean and unitary standard deviation by construction and the random permutation makes them independent. Consider now the matrix

$$\mathbf{T} = \mathbf{KC} \tag{31}$$

and note that, according to equations (28) and (29), $\mathbf{T}$ has a linear correlation matrix equal to the target correlation matrix $\mathbf{S}$:

$$\mathbf{R}_{lin}(\mathbf{T}) = n^{-1}\mathbf{T}^T\mathbf{T} = \mathbf{C}^T \underbrace{n^{-1}\mathbf{K}^T\mathbf{K}}_{\mathbf{I}}\mathbf{C} = \mathbf{S}. \tag{32}$$

The basis of the IC method is as follows: generate the matrix $\mathbf{T}$ as explained above and then produce a new matrix $\mathbf{X}$ which is a rearranged version of $\mathbf{X}_{in}$ so that its samples have the same ranking position of the corresponding samples of $\mathbf{T}$. With reference to Fig. 6, note that the matrix $\mathbf{T}$ depends on the correlation matrix we want to induce and on the "scores matrix" $\mathbf{K}$ which is deterministic. So, it does not have to be evaluated during simulation runs, i.e., it may be computed *offline*. The only operation which must be executed in real time is the generation and the rearrangement of $\mathbf{X}$, which is not computationally expensive.

A scheme explaining how the rank matching between matrices $\mathbf{T}$ and $\mathbf{X}$ is carried out column by column is shown in Fig. 7.

At this point two observations are necessary:

• The *rank* correlation matrix of the rearranged data $\mathbf{R}_{rank}(\mathbf{X})$ will match exactly $\mathbf{R}_{rank}(\mathbf{T})$ and though $\mathbf{T}$ is constructed so that $\mathbf{R}_{lin}(\mathbf{T}) = \mathbf{S}$, the rank correlation matrix $\mathbf{R}_{rank}(\mathbf{T})$ is also close to $\mathbf{S}$. This happens because when there are no prominent outliers, as is the
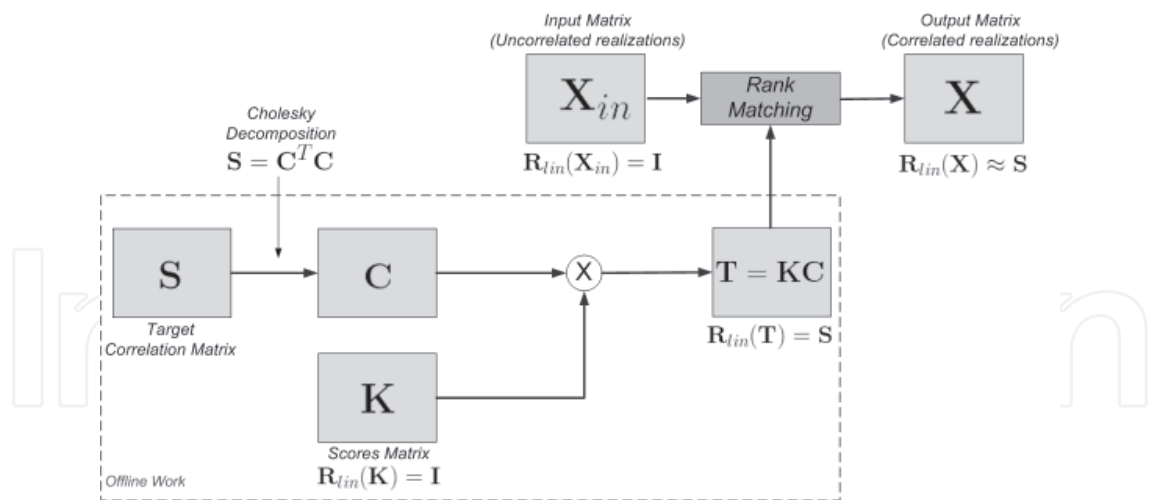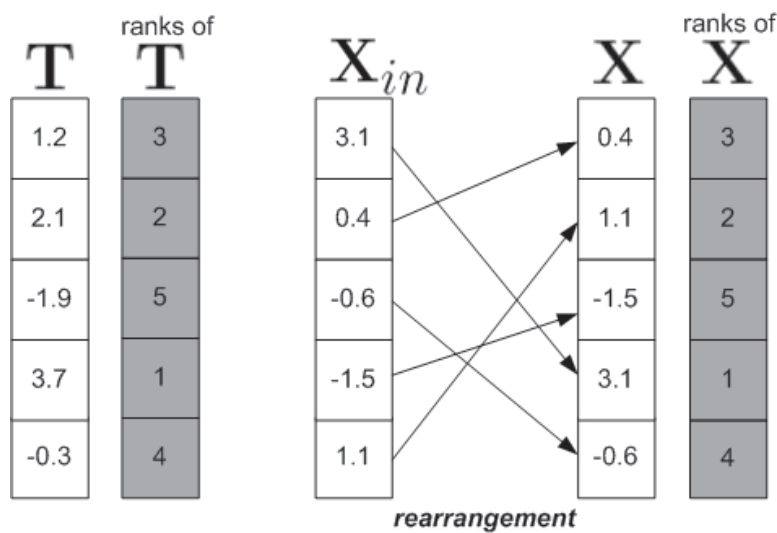
Fig. 6. Block diagram of the IC method.

Fig. 7. Rank matching.

   case of $\mathbf{T}$ whose column elements are normally distributed, linear and rank correlation coefficients are very close to each other and so $\mathbf{R}_{rank}(\mathbf{T}) \approx \mathbf{R}_{lin}(\mathbf{T}) = \mathbf{S}$. Moreover, for WSS processes we may expect $\mathbf{R}_{lin}(\mathbf{X}) \approx \mathbf{R}_{rank}(\mathbf{X})$ (Lehmann & D'Abrera, 1975) and, since $\mathbf{R}_{rank}(\mathbf{X}) = \mathbf{R}_{rank}(\mathbf{T}) \approx \mathbf{R}_{lin}(\mathbf{T}) = \mathbf{S}$, then $\mathbf{R}_{lin}(\mathbf{X}) \approx \mathbf{S}$.

- Row-wise, the permutation resulting from the rearrangement of $\mathbf{X}$ appears random and thus the n samples in any given column remain uncorrelated.

The rearrangement of the input matrix $\mathbf{X}$ is carried out according to a ranking matrix which is *directly* derived from the desired correlation matrix and this operation does not affect the input marginal distributions. This means that it is possible to induce arbitrary (rank) correlations between vectors with arbitrary distributions, a fundamental task in fading channel simulation. In the sequel we analyze the effects of the finite sample size error and its compensation.

As introduced above, the linear correlation matrix of $\mathbf{T} = \mathbf{KC}$ is, by construction, equal to $\mathbf{S}$. However, due to finite sample size, a small error can be introduced in the simulation by the non-perfect independence of the columns of $\mathbf{K}$. This error can be corrected with an adjustment proposed by the authors of this method in (Iman & Conover, 1982). Consider that $\mathbf{E} = \mathbf{R}_{lin}(\mathbf{K})$

is the correlation matrix of $\mathbf{K}$ and that it allows a Cholesky decomposition $\mathbf{E} = \mathbf{F}^T\mathbf{F}$. We have verified that for $\mathbf{K}$ constructed as in (30), $\mathbf{E}$ is generally very close to positive-definite. In some cases however, a regularization step may be required, by adding a small $\delta > 0$ to each element in the main diagonal of $\mathbf{E}$. This does not sacrifice accuracy because δ is very small. Following the rationale above, if the matrix $\mathbf{T}$ is now constructed such that $\mathbf{T} = \mathbf{K}\mathbf{F}^{-1}\mathbf{C}$, then it has covariance matrix

$$\frac{1}{n}\mathbf{T}^T\mathbf{T} = \mathbf{C}^T\mathbf{F}^{-T}\underbrace{\mathbf{K}^T\mathbf{K}}_{\mathbf{E}=\mathbf{F}^T\mathbf{F}}\mathbf{F}^{-1}\mathbf{C} = \mathbf{C}^T\underbrace{\mathbf{F}^{-T}\mathbf{F}^T}_{\mathbf{I}}\underbrace{\mathbf{F}\mathbf{F}^{-1}}_{\mathbf{I}}\mathbf{C} = \mathbf{C}^T\mathbf{C} = \mathbf{S} \tag{33}$$

as desired. In (33), the notation $\mathbf{F}^{-T}$ stands for the inverse of the transpose of $\mathbf{F}$. With this adjustment, a possible error introduced by the non-perfect independence of the columns of $\mathbf{K}$ is completely canceled.

With the goal of quantifying the gain obtained with this adjustment it is possible to calculate the MSE between the output linear correlation matrix $\mathbf{R}_{lin}(\mathbf{X})$ and the target $\mathbf{S}$ with and without the error compensation. We define the matrix $\mathbf{D} \triangleq \mathbf{R}_{lin}(\mathbf{X}) - \mathbf{S}$ and the MSE as

$$\text{MSE} = \frac{1}{MN}\sum_{i=1}^{M}\sum_{j=1}^{N} d_{ij}^2 \tag{34}$$

where d_{ij} is the element of $\mathbf{D}$ with row index i and column index j.

4.1 Using the Iman-Conover method for the simulation of MIMO and SISO channels

Let us consider the MIMO propagation scenario depicted in Fig. 8, with M transmitting antennas at the Base Station (BS) and N receiving antennas at the Mobile Station (MS). Considering all possible combinations, the MIMO channel can be subdivided into MN subchannels. Moreover, due to multipath propagation, each subchannel is composed by L uncorrelated paths. In general these paths are complex-valued. For simplicity we will consider that these paths are real-valued (in-phase component only) but the generalization of the method for complex paths is straightforward. The IC method can be used for MIMO channels simulation by simply storing the MIMO channel samples in a $n \times MNL$ matrix $\mathbf{X}_{in}$, where MNL is the number of subchannels considering multipath and n is the number of samples generated for each subchannel. The target (desired) spatial correlation coefficients of the MIMO channel are stored in a $MNL \times MNL$ symmetric positive definite matrix $\mathbf{S}_{MIMO}$ (Petrolino & Tavares, 2010a). After this, the application of the IC method to matrix $\mathbf{X}_{in}$, will produce a new matrix $\mathbf{X}$. The columns of $\mathbf{X}$ contain the subchannels realizations which are spatially correlated according to the desired correlation coefficients in $\mathbf{S}_{MIMO}$ and whose PDFs are preserved.

We have also used the IC method for the simulation of SISO channels. This idea comes from the following observation. As the final result of the IC method we have a rearranged version of the input matrix $\mathbf{X}_{in}$, so that its columns are correlated as desired. This means that if we extract any row from this matrix, the samples therein are correlated according to the ACF contained in the $P \times P$ target correlation matrix $\mathbf{S}_{SISO}$ (Petrolino & Tavares, 2010b). Note also that for stationary processes, $\mathbf{S}_{SISO}$ is Toeplitz so all rows will exhibit the same ACF.

If we consider P as the number of correlated samples to be generated with the IC method and n as the number of uncorrelated fading realizations (often required when Monte Carlo simulations are necessary), after the application of the IC method we obtain a $n \times P$ matrix $\mathbf{X}$ whose correlation matrix is equal to the target $\mathbf{S}_{SISO}$. Its n rows are uncorrelated and each contains a P-samples fading sequence with the desired ACF. These n columns can be extracted and used for Monte Carlo simulation of SISO channels.
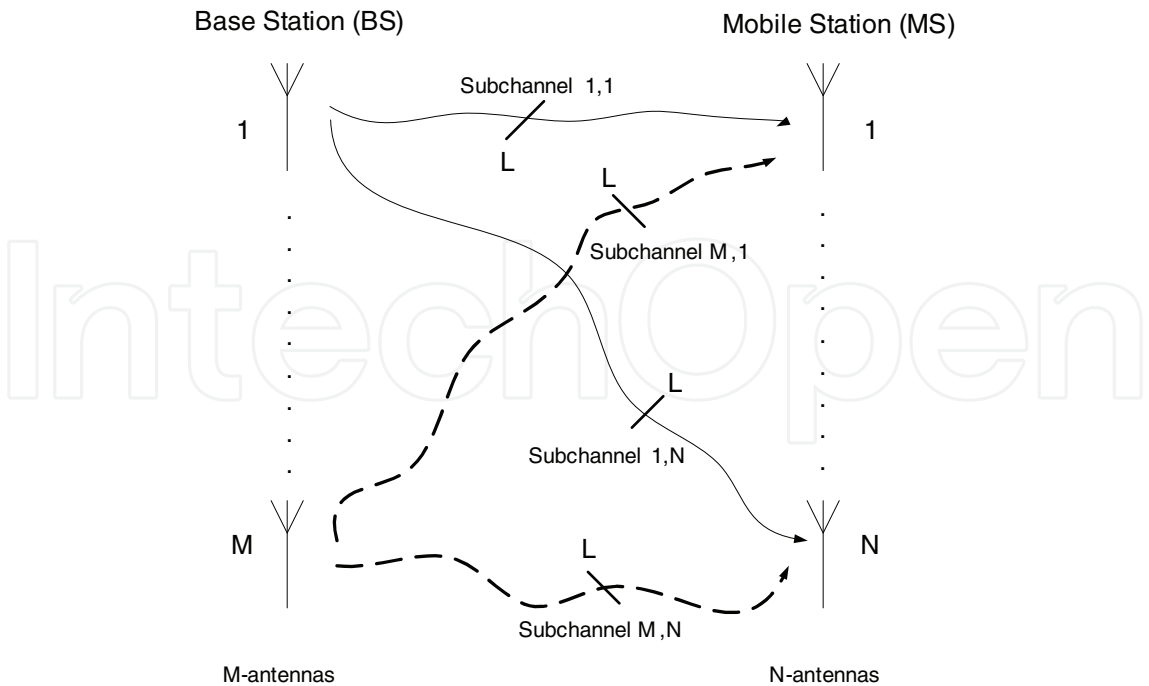
Fig. 8. Propagation scenario for multipath MIMO channels.

5. Simulation of MIMO and SISO channels with the IC method

In this Section we present results obtained by applying the IC method to the simulation of different MIMO and SISO channels [2]. The MH candidate pairs are jointly Gaussian distributed with zero mean and a variance which is set depending on the target density. The constant K introduced in equation (16) has been adjusted by experimentation to achieve an acceptance rate of about 50%.

5.1 Simulation of a 2×1 MIMO channel affected by Rayleigh fading

Let us first consider a scenario with $M = 2$ antennas at the BS and $N = 1$ antennas at the MS. For both subchannels, multipath propagation exists but, for simplicity, the presence of only 2 paths per subchannel ($L = 2$) is considered. This means that the channel matrix $\mathbf{X}$ is $n \times 4$, where n is the number of generated samples. Equi-spaced antenna elements are considered at both ends with half a wavelength element spacing. We consider the case of no local scatterers close to the BS as usually happens in typical urban environments and the power azimuth spectrum (PAS) following a Laplacian distribution with a mean azimuth spread (AS) of $10°$. Given these conditions, an analytical expression for the spatial correlation at the BS is given in (Pedersen et al., 1998, eq.12), which leads to

$$\mathbf{S}_{BS} = \begin{bmatrix} 1 & 0.874 \\ 0.874 & 1 \end{bmatrix}. \tag{35}$$

Since $N = 1$, the correlation matrix collapses into an autocorrelation coefficient at the MS, i.e.,

$$\mathbf{S}_{MS} = 1. \tag{36}$$

---

[2] In the following examples, the initial uncorrelated Nakagami-m, Weibull and Hoyt rvs have been generated using the MH algorithm described in Sections 2 and 3.

Remembering that $\mathbf{S}_{MIMO} = \mathbf{S}_{BS} \otimes \mathbf{S}_{MS}$, we have an initial correlation matrix

$$\mathbf{S}_{MIMO} = \begin{bmatrix} 1 & 0.874 \\ 0.874 & 1 \end{bmatrix}. \tag{37}$$

Equation (37) represents the spatial correlation existing between the subchannel paths at any time delay. If we remember that in this example we are considering $L = 2$ paths for each subchannel, recalling that non-zero correlation coefficients exist only between paths which are referred to the same path delay, we obtain the final zero-padded spatial correlation matrix $\mathbf{S}_{MIMO}$ as

$$\mathbf{S}_{MIMO} = \begin{bmatrix} 1 & 0.874 & 0 & 0 \\ 0.874 & 1 & 0 & 0 \\ 0 & 0 & 1 & 0.874 \\ 0 & 0 & 0.874 & 1 \end{bmatrix}. \tag{38}$$

As is done in most studies (Gesbert et al., 2000), the subchannel samples are considered as realizations of uncorrelated Gaussian rvs. In the following examples a sample length of $n = 100000$ samples has been chosen. Since very low values of the MSE in (34) are achieved for large n, simulations have been run without implementing the error compensation discussed in the previous Section. The simulated spatial correlation matrix $\hat{\mathbf{S}}_{MIMO}$ is

$$\hat{\mathbf{S}}_{MIMO} = \begin{bmatrix} 1.0000 & 0.8740 & -0.0000 & -0.0001 \\ 0.8740 & 1.0000 & -0.0000 & -0.0001 \\ -0.0000 & -0.0000 & 1.0000 & 0.8740 \\ -0.0001 & -0.0001 & 0.8740 & 1.0000 \end{bmatrix}. \tag{39}$$

The comparison between (38) and (39) demonstrates the accuracy of the proposed method. The element-wise absolute difference between $\hat{\mathbf{S}}_{MIMO}$ and $\mathbf{S}_{MIMO}$ is of the order of 10^{-4}.

5.2 Simulation of a 2×3 MIMO channel affected by Rayleigh, Weibull and Nakagami-m fading
We now present a set of results to show that the IC method is distribution-free, which means that the subchannels marginal PDFs are preserved. For this reason we simulate a single-path ($L = 1$) 2×3 MIMO system and consider that the subchannel envelopes arriving at the first Rx antenna are Rayleigh, those getting the second antenna are Weibull distributed with a fading severity parameter $\beta = 1.5$ (fading more severe than Rayleigh) and finally those arriving at the third one are Nakagami-m distributed with $m = 3$ (fading less severe than Rayleigh). In the first two cases the phases are considered uniform in $[0, 2\pi)$, while in the case of Nakagami envelope, the corresponding phase distribution (Yacoub et al., 2005, eq. 3) is also considered. For the sake of simplicity, from now on only the real part of the processes are considered. Being the real and imaginary parts of the considered processes equally distributed, the extension of this example to the imaginary components is straightforward. The Rayleigh envelope and uniform phase leads to a Gaussian distributed in-phase component[3] $f_{X_r}(x_r)$ for subchannels $\mathbf{H}_{1,1}$ and $\mathbf{H}_{2,1}$. The in-phase component PDF $f_{X_w}(x_w)$ of subchannels $\mathbf{H}_{1,2}$ and $\mathbf{H}_{2,2}$ has been obtained by transformation of the envelope and phase rvs into their corresponding in-phase and quadrature (IQ) components rvs. It is given by

$$f_{X_w}(x_w) = \int_{-\infty}^{\infty} f_{X_w Y_w}(x_w, y_w) dy_w \tag{40}$$

---

[3] In the following, the subscripts r, w and n refer to the fading distribution (Rayleigh, Weibull and Nakagami-m) in the respective subchannels.

where

$$f_{X_w Y_w}(x_w, y_w) = \frac{\beta}{2\pi\Omega_w}(x_w^2 + y_w^2)^{\frac{\beta-2}{2}} \exp\left(-\frac{(x_w^2 + y_w^2)^{\frac{\beta}{2}}}{\Omega_w}\right) \tag{41}$$

is the IQ components joint PDF obtained considering a Weibull distributed envelope and uniform phase in $[0, 2\pi]$ and where Ω_w is the average fading power. Finally, the in-phase PDF $f_{X_n}(x_n)$ for subchannels $\mathbf{H}_{1,3}$ and $\mathbf{H}_{2,3}$ is obtained by integrating the IQ joint PDF corresponding to the Nakagami-m fading. It has been deduced by transformation of the envelope and phase rvs, whose PDFs are known (Yacoub et al., 2005), into their corresponding IQ components rvs. It is given by

$$f_{X_n Y_n}(x_n, y_n) = \frac{m^m |\sin(2\theta)|^{m-1}\rho^{2m-2}}{2^{m-1}\Omega_n^m \Gamma^2(m/2)} \exp\left(-\frac{m\rho^2}{\Omega_n}\right) \tag{42}$$

where $\rho = \sqrt{x_n^2 + y_n^2}$, $\theta = \tan^{-1}(y_n/x_n)$, $\Gamma(\cdot)$ is the Gamma function and Ω_n is the average fading power. At the BS, the same conditions of the previous examples are considered, except for the antenna separation which in this case is chosen to be one wavelength. Given these conditions, the spatial correlation matrix at the BS is

$$\mathbf{S}_{BS} = \begin{bmatrix} 1 & 0.626 \\ 0.626 & 1 \end{bmatrix}. \tag{43}$$

Note that, due to the larger antenna separation, the spatial correlation between the antennas at the BS is lower than in the previous examples, where a separation of half a wavelength has been considered. Also at the MS, low correlation coefficients between the antennas are considered. This choice is made with the goal of making this scenario (with three different distributions) more realistic. Hence, we assume

$$\mathbf{S}_{MS} = \begin{bmatrix} 1 & 0.20 & 0.10 \\ 0.20 & 1 & 0.20 \\ 0.10 & 0.20 & 1 \end{bmatrix}. \tag{44}$$

It follows that
$$\mathbf{S}_{MIMO} =$$
$$\begin{bmatrix} 1 & 0.2000 & 0.1000 & 0.6268 & 0.1254 & 0.0627 \\ 0.2000 & 10.2000 & 0.1254 & 0.6268 & 0.1254 & \\ 0.1000 & 0.2000 & 1 & 0.0627 & 0.1254 & 0.6268 \\ 0.6268 & 0.1254 & 0.0627 & 1 & 0.2000 & 0.1000 \\ 0.1254 & 0.6268 & 0.1254 & 0.2000 & 1 & 0.2000 \\ 0.0627 & 0.1254 & 0.6268 & 0.1000 & 0.2000 & 1 \end{bmatrix}. \tag{45}$$

The simulated correlation matrix is

$$\hat{\mathbf{S}}_{MIMO} =$$
$$\begin{bmatrix} 1.0000 & 0.1974 & 0.0995 & 0.6268 & 0.1238 & 0.0623 \\ 0.1974 & 1.0000 & 0.1961 & 0.1240 & 0.6144 & 0.1229 \\ 0.0995 & 0.1961 & 1.0000 & 0.0623 & 0.1227 & 0.6209 \\ 0.6268 & 0.1240 & 0.0623 & 1.0000 & 0.1973 & 0.0994 \\ 0.1238 & 0.6144 & 0.1227 & 0.1973 & 1.0000 & 0.1956 \\ 0.0623 & 0.1229 & 0.6209 & 0.0994 & 0.1956 & 1.0000 \end{bmatrix}. \tag{46}$$

Also in this case the simulated spatial correlation matrix provides an excellent agreement with the target correlation as is seen from the comparison between (45) and (46). Figs. 9, 10 and 11 demonstrate that the application of the proposed method does not affect the subchannels PDF. After the simulation run the agreement between the theoretical marginal distribution (evaluated analytically) and the generated samples histogram is excellent.
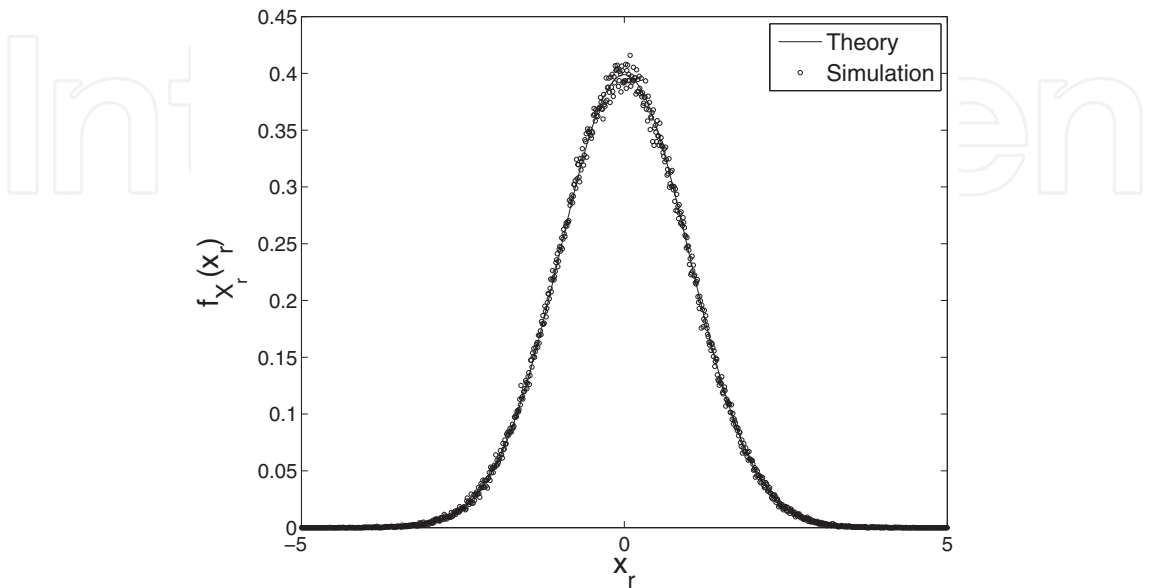

Fig. 9. PDF of the in-phase component for subchannels $\mathbf{H}_{1,1}$ and $\mathbf{H}_{2,1}$ affected by Rayleigh fading after the application of the method, plotted against the theoretical reference.
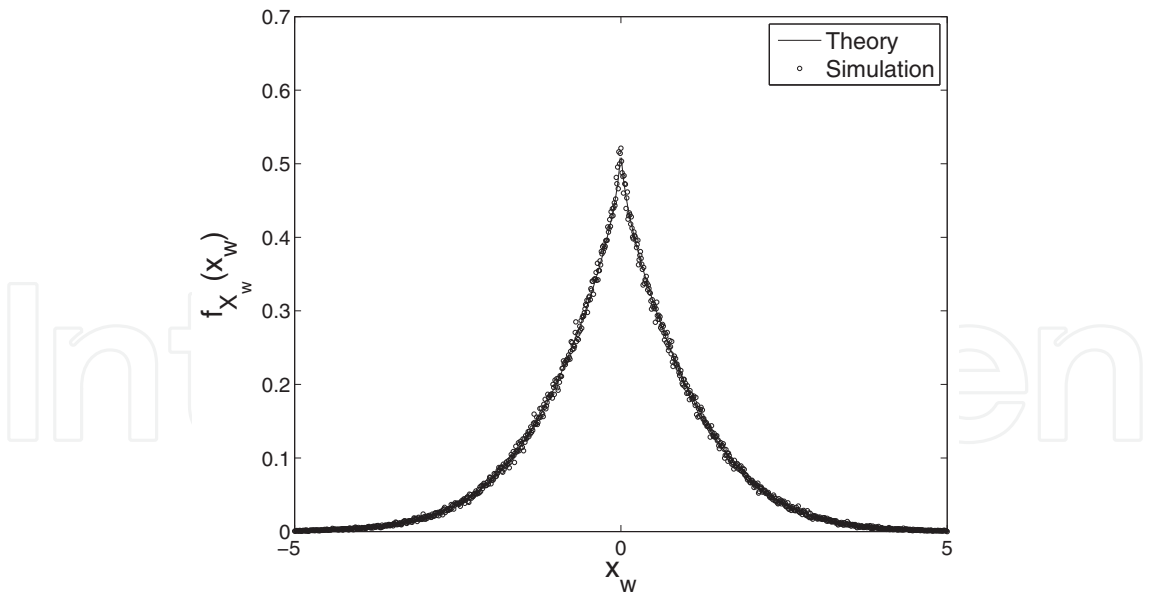
Fig. 10. PDF of the in-phase component for subchannels $\mathbf{H}_{1,2}$ and $\mathbf{H}_{2,2}$ affected by Weibull ($\beta = 1.5$) fading after the application of the method, plotted against the theoretical reference.

5.3 SISO fading channel simulation with the IC method

The use of non-Rayleigh envelope fading PDFs has been gaining considerable success and acceptance in the last years. Experience has indeed shown that the Rayleigh distribution
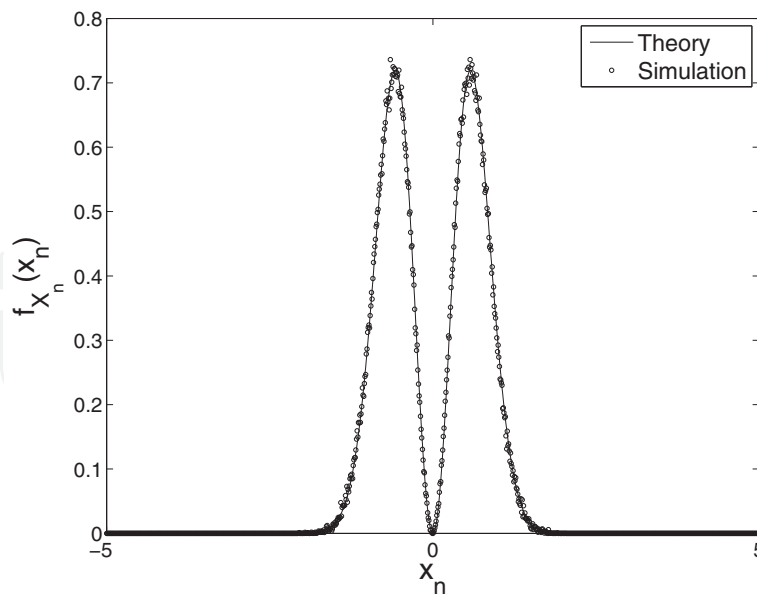
Fig. 11. PDF of the in-phase component for subchannels $\mathbf{H}_{1,3}$ and $\mathbf{H}_{2,3}$ affected by Nakagami-m ($m = 3$) fading after the application of the method, plotted against the theoretical reference.

shows a good matching with real fadings only in particular cases of fading severity. More general distributions (e.g., the Nakagami-m and Weibull) allow a convenient channel severity to be set simply by tuning one parameter and are advisable for modeling a larger class of fading envelopes. As reported in the Introduction, in the case of Rayleigh fading, according to the model of Clarke, the fading process $h(t)$ is modeled as a complex Gaussian process with independent real and imaginary parts $h_R(t)$ and $h_I(t)$ respectively. In the case of isotropic scattering and omni-directional receiving antennas, the normalized ACF of the quadrature components is given by (5). An expression for the normalized ACF of the Rayleigh envelope process $r(t) = \sqrt{h_R^2(t) + h_I^2(t)}$ can be found in (Jakes, 1974). It is given by

$$\mathcal{R}_r(\tau) = {}_2F_1\left[-\frac{1}{2}, -\frac{1}{2}; 1; J_0^2(2\pi f_D \tau)\right] \qquad (47)$$

where ${}_2F_1(\cdot, \cdot; \cdot; \cdot)$ is a Gauss hypergeometric function.

In this Section we present the results obtained by using the IC method for the direct simulation of correlated Nakagami-m and Weibull envelope sequences (Petrolino & Tavares, 2010b). In particular, the simulation problem has been approached as follows: uncorrelated envelope fading sequences have been generated with the MH algorithm and the IC method has been afterwards applied to the uncorrelated sequences with the goal of imposing the desired correlation structure, derived from existing channel models. Since the offline part of the IC method has been discussed in the previous Section, here we present the online part for the simulation of SISO channels. So, from now on, we consider that a matrix $\mathbf{T}_{rank}$, containing the ranking positions of the matrix $\mathbf{T}$ has been previously computed and is available. Recalling the results of Section 4, there are only two operations that must be executed during the online simulation run:

1. Generate the $n \times P$ input matrix $\mathbf{X}_{in}$ containing nP uncorrelated rvs with the desired PDF.

2. Create matrix $\mathbf{X}$ which is a rearranged version of $\mathbf{X}_{in}$ according to the ranks contained in $\mathbf{T}_{rank}$ to get the desired ACF.

Each of the n rows of $\mathbf{X}$ represents an P-samples fading sequence which can be used for channel simulation.

5.3.1 Simulation of a SISO channel affected by Nakagami-m fading

In 1960, M. Nakagami proposed a PDF which models well the signal amplitude fading in a large range of propagation scenarios. A rv R_N is Nakagami-m distributed if its PDF follows the distribution (Nakagami, 1960)

$$f_{R_N}(r) = \frac{2m^m r^{2m-1}}{\Gamma(m)\Omega^m} \exp\left(-\frac{mr^2}{\Omega}\right), \quad r \geq 0, \ m > \frac{1}{2} \tag{48}$$

where $\Gamma(\cdot)$ is the gamma function, $\Omega = \mathbb{E}[R_N^2]$ is the mean power and $m = \Omega^2/(R_N^2 - \Omega)^2 \geq \frac{1}{2}$ is the Nakagami-m fading parameter which controls the depth of the fading amplitude.

For $m = 1$ the Nakagami model coincides with the Rayleigh model, while values of $m < 1$ correspond to more severe fading than Rayleigh and values of $m > 1$ to less severe fading than Rayleigh. The Nakagami-m envelope ACF is found as (Filho et al., 2007)

$$R_{R_N}(\tau) = \frac{\Omega\Gamma^2(m + \frac{1}{2})}{m\Gamma^2(m)} {}_2F_1\left[-\frac{1}{2}, -\frac{1}{2}; \ m; \rho(\tau)\right] \tag{49}$$

where $\rho(\tau)$ is an autocorrelation coefficient (ACC) which depends on the propagation scenario. In this example and without loss of generality, we consider the isotropic scenario with uniform distributed waves angles of arrival for which $\rho(\tau) = J_0^2(2\pi f_D \tau)$. With the goal of reducing the simulation error induced by the finiteness of the sample size n, the simulated ACF has been evaluated on all the n rows of the rearranged matrix $\mathbf{X}$ and finally the arithmetic mean has been taken. Fig. 12 shows the results of the application of the proposed method to the generation of correlated Nakagami-m envelope sequences. As is seen, the simulated ACF matches the theoretical reference very well.

5.3.2 Simulation of a SISO channel affected by Weibull fading

The Weibull distribution is one of the most used PDFs for modeling the amplitude variations of the fading processes. Indeed, field trials show that when the number of radio wave paths is limited the variation in received signal amplitude frequently follows the Weibull distribution (Shepherd, 1977). The Weibull PDF for a rv R_W is given by (Sagias et al., 2004)

$$f_{R_W}(r) = \frac{\beta r^{\beta-1}}{\Omega} \exp\left(-\frac{r^\beta}{\Omega}\right) \quad r, \beta \geq 0 \tag{50}$$

where $\mathbb{E}[r^\beta] = \Omega$ and β is the fading severity parameter. As the value of β increases, the severity of the fading decreases, while for the special case of $\beta = 2$ the Weibull PDF reduces to the Rayleigh PDF (Sagias et al., 2004).

The Weibull envelope ACF has been obtained in (Yacoub et al., 2005) and validated by field trials in (Dias et al., 2005). Considering again an isotropic scenario as was done in the case of Nakagami fading, it is given by
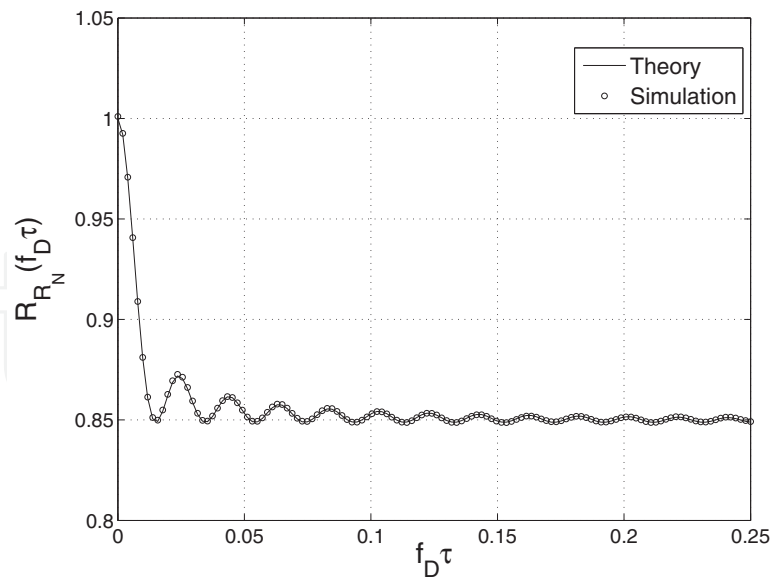
Fig. 12. Normalized linear ACF of the simulated Nakagami-m fading process plotted against the theoretical normalized ACF for $m = 1.5$, normalized Doppler frequency $f_D = 0.05$, $n = 10000$ realizations and $P = 2^{10}$ samples.
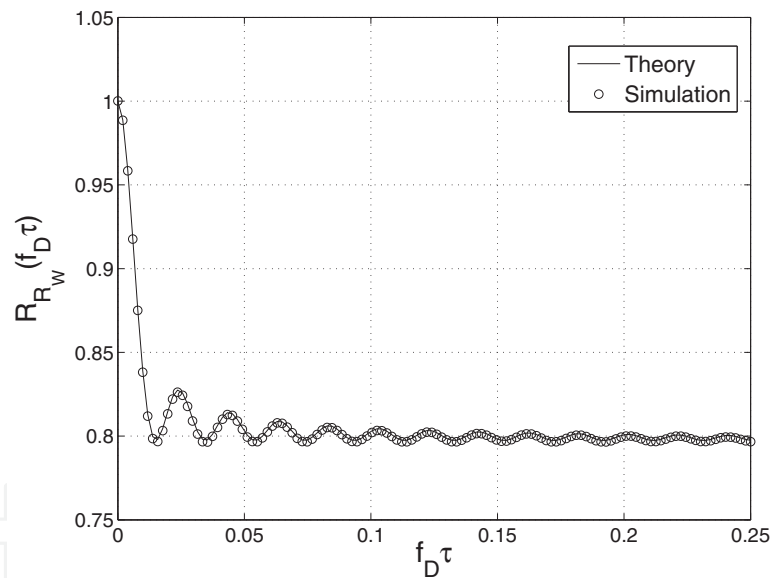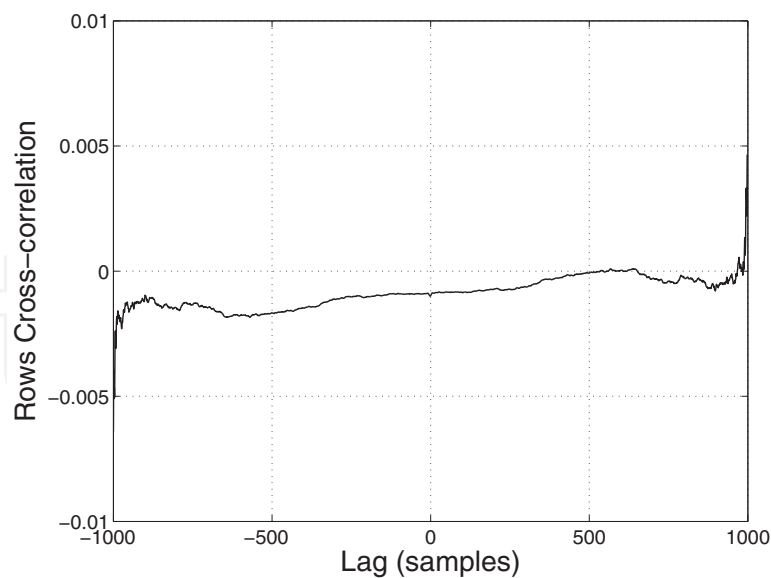

Fig. 13. Normalized linear ACF of the simulated Weibull fading process plotted against the theoretical normalized ACF for $\beta = 2.5$, normalized Doppler frequency $f_D = 0.05$, $n = 10000$ realizations and $P = 2^{10}$ samples.

$$R_{R_W}(\tau) = \Omega^{2/\beta} \Gamma^2 \left(1 + \frac{1}{\beta}\right) {}_2F_1 \left[-\frac{1}{\beta}, -\frac{1}{\beta}; 1; J_0^2(2\pi f_D \tau)\right]. \tag{51}$$

Also in this example an isotropic scenario with uniform distributed waves angles of arrival is considered. The simulated ACF has been evaluated on all the n rows of the rearranged matrix $\mathbf{X}$ and finally the arithmetic mean has been taken. Fig. 13 shows the results of the application of the proposed method to the generation of correlated Weibull envelope

Fig. 14. Average row crosscorrelation of the simulated Weibull fading process for $\beta = 2.5$, normalized Doppler frequency $f_D = 0.05$, $n = 1000$ realizations and $P = 2^{10}$ samples.

sequences. The simulated ACF matches the theoretical reference quite well. Fig. 14 plots the average row crosscorrelation obtained from a simulation run of a Weibull fading process with autocorrelation (51), for $n = 1000$ realizations and $P = 2^{10}$ samples. As is seen, the crosscorrelation between rows is quite small (note the scale). This means that the n realizations produced by the method are statistically uncorrelated, as is required for channel simulation.

6. Conclusions

In this chapter, we presented a SISO and MIMO fading channel simulator based on the Iman-Conover (IC) method (Iman & Conover, 1982). The method allows the simulation of radio channels affected by arbitrarily distributed fadings. The method is distribution-free and is able to induce any desired spatial correlation matrix in case of MIMO simulations (Petrolino & Tavares, 2010a) and any time ACF in case of SISO channels (Petrolino & Tavares, 2010b), while preserving the initial PDF of the samples. The proposed method has been applied in different MIMO and SISO scenarios and has been shown to provide excellent results. We have also presented a simulator for Gaussian-based fading processes, like Rayleigh and Rician fading. These simulators are based on the Karhunen-Loève expansion and have been applied to the simulation of mobile-to-fixed (Petrolino et al., 2008a) and mobile-to-mobile (Petrolino et al., 2008b) fading channels. Moreover a technique for generating uncorrelated arbitrarily distributed sequences has been developed with the goal of combining it with the IC method. This technique is based on the Metropolis-Hastings algorithm (Hastings, 1970; Metropolis et al., 1953) and allows the application of the IC method to a larger class of fadings.

7. References

Beaulieu, N. & Cheng, C. (2001). An efficient procedure for Nakagami-m fading simulation, *Global Telecommunications Conf., 2001. GLOBECOM '01. IEEE*, Vol. 6, pp. 3336–3342.

Chib, S. & Greenberg, E. (1995). Understanding the Metropolis-Hastings algorithm, *The American Statistician* 49(4): 327–335.

Clarke, R. H. (1968). A statistical theory of mobile-radio reception, *Bell Systems Tech. Jou.* 47(6): 957–1000.

Dias, U., Fraidenraich, G. & Yacoub, M. (2005). On the Weibull autocorrelation function: field trials and validation, *Microwave and Optoelectronics, 2005 SBMO/IEEE MTT-S International Conference on*, pp. 505–507.

Filho, J., Yacoub, M. & Fraidenraich, G. (2007). A simple accurate method for generating autocorrelated Nakagami-*m* envelope sequences, *IEEE Comm. Lett.* 11(3): 231–233.

Gesbert, D., Bolcskei, H., Gore, D. & Paulraj, A. (2000). MIMO wireless channels: capacity and performance prediction, *Global Telecommunications Conference, 2000. GLOBECOM '00. IEEE*, Vol. 2, pp. 1083–1088.

Hastings, W. K. (1970). Monte Carlo sampling methods using Markov chains and their applications, *Biometrika* 57(1): 97–109.

Hoyt, R. (1947). Probability functions for the modulus and angle of the normal complex variate, *Bell System Technical Journal* 26: 318–359.

Iman, R. & Conover, W. (1982). A distribution-free approach to inducing rank correlation among input variables, *Communications in Statistics-Simulation and Computation* 11: 311–334.

Jakes, W. C. (1974). *Microwave Mobile Communications*, John Wiley & Sons, New York.

Komninakis, C. (2003). A fast and accurate Rayleigh fading simulator, *Global Telecommunications Conference, 2003. GLOBECOM '03. IEEE* 6: 3306–3310.

Lehmann, E. L. & D'Abrera, H. J. M. (1975). *Nonparametrics: Statistical Methods Based on Ranks*, McGraw-Hill, New York.

Metropolis, N., Rosenbluth, A. W., Rosenbluth, M. N., Teller, A. H. & Teller, E. (1953). Equation of state calculations by fast computing machines, *The Journal of Chemical Physics* 21(6): 1087–1092.

Nakagami, N. (1960). The *m*-distribution, a general formula for intensity distribution of rapid fading, *in* W. G. Hoffman (ed.), *Statistical Methods in Radio Wave Propagation*, Oxford, England: Pergamon.

Patel, C., Stuber, G. & Pratt, T. (2005). Simulation of Rayleigh-faded mobile-to-mobile communication channels, *IEEE Trans. on Comm.* 53(11): 1876–1884.

Pätzold, M. (2002). *Mobile Fading Channels*, John Wiley & Sons, New York.

Pätzold, M., Killat, U., Laue, F. & Li, Y. (1998). On the statistical properties of deterministic simulation models for mobile fading channels, *IEEE Trans. on Veh. Tech.* 47(1): 254–269.

Pedersen, K., Mogensen, P. & Fleury, B. (1998). Spatial channel characteristics in outdoor environments and their impact on BS antenna system performance, *IEEE 48th Vehicular Technology Conference, 1998. VTC 98*, Vol. 2, pp. 719–723.

Petrolino, A., Gomes, J. & Tavares, G. (2008a). A fading channel simulator based on a modified Karhunen-Loève expansion, *Radio and Wireless Symposium, 2008 IEEE*, Orlando (FL), USA, pp. 101 –104.

Petrolino, A., Gomes, J. & Tavares, G. (2008b). A mobile-to-mobile fading channel simulator based on an orthogonal expansion, *IEEE 67th Vehicular Technology Conference: VTC2008-Spring*, Marina Bay, Singapore, pp. 366 –370.

Petrolino, A. & Tavares, G. (2010a). Inducing spatial correlation on MIMO channels: a distribution-free efficient technique, *IEEE 71st Vehicular Technology Conference: VTC2010-Spring*, Taipei, Taiwan, pp. 1–5.

Petrolino, A. & Tavares, G. (2010b). A simple method for the simulation of autocorrelated and arbitrarily distributed envelope fading processes, *IEEE International Workshop on Signal Processing Advances in Wireless Communications.*, Marrakech, Morocco.

Pop, M. & Beaulieu, N. (2001). Limitations of sum-of-sinusoids fading channel simulators, *IEEE Trans. on Comm.* 49(4): 699–708.

Sagias, N., Zogas, D., Karagiannidis, G. & Tombras, G. (2004). Channel capacity and second-order statistics in Weibull fading, *IEEE Comm. Lett.* 8(6): 377–379.

Shepherd, N. (1977). Radio wave loss deviation and shadow loss at 900 MHz, *IEEE Trans. on Veh. Tech.* 26(4): 309–313.

Smith, J. I. (1975). A computer generated multipath fading simulation for mobile radio, *IEEE Trans. on Veh. Tech.* 24(3): 39–40.

Tierney, L. (1994). Markov chains for exploring posterior distributions, *Annals of Statistics* 22(4): 1701–1728.

Van Trees, H. L. (1968). *Detection, Estimation, and Modulation Theory - Part I*, Wiley, New York.

Vehicular Technology Society Committee on Radio Propagation (1988). Coverage prediction for mobile radio systems operating in the 800/900 MHz frequency range, *IEEE Trans. on Veh. Tech.* 37(1): 3–72.

Wang, C. (2006). Modeling MIMO fading channels: Background, comparison and some progress, *Communications, Circuits and Systems Proceedings, 2006 International Conference on*, Vol. 2, pp. 664–669.

Weibull, W. (1951). A statistical distribution function of wide applicability, *ASME Jou. of Applied Mechanics, Trans. of the American Society of Mechanical Engineers* 18(3): 293–297.

Yacoub, M., Fraidenraich, G. & Santos Filho, J. (2005). Nakagami-*m* phase-envelope joint distribution, *Electr. Lett.* 41(5): 259–261.

Young, D. & Beaulieu, N. (2000). The generation of correlated Rayleigh random variates by inverse discrete Fourier transform, *IEEE Trans. on Comm.* 48(7): 1114–1127.
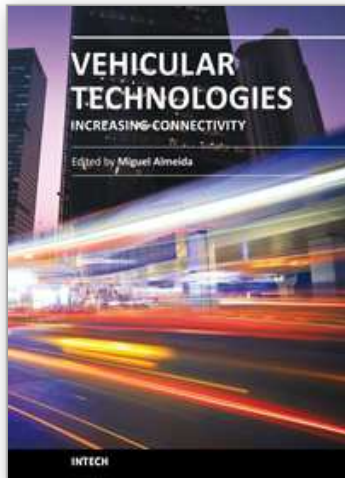
Vehicular Technologies: Increasing Connectivity

Edited by Dr Miguel Almeida

ISBN 978-953-307-223-4

Hard cover, 448 pages

Publisher InTech

Published online 11, April, 2011

Published in print edition April, 2011

This book provides an insight on both the challenges and the technological solutions of several approaches, which allow connecting vehicles between each other and with the network. It underlines the trends on networking capabilities and their issues, further focusing on the MAC and Physical layer challenges. Ranging from the advances on radio access technologies to intelligent mechanisms deployed to enhance cooperative communications, cognitive radio and multiple antenna systems have been given particular highlight.